Eur. Phys. J. D **29**, 69–76 (2004)
DOI: 10.1140/epjd/e2004-00004-8

THE EUROPEAN PHYSICAL JOURNAL D

Hydrodynamic simulation of XUV laser-produced plasmas

M. Fajardo[1,a], P. Zeitoun[2], and J.-C. Gauthier[3]

[1] Centro de Física de Plasmas, Instituto Superior Técnico, 1049-001 Lisbon, Portugal
[2] Laboratoire d'Interaction du Rayonnement X avec la Matière, Université Paris-Sud, 91405 Orsay, France
[3] Centre Lasers Intenses et Applications, UMR 5107 du CNRS, Université Bordeaux I, CEA, Université Bordeaux I, 33405 Talence, France

Received 7 October 2003 / Received in final form 6 December 2003
Published online 20 January 2004 –

Abstract. With the construction of novel XUV sources, such as VUV FEL's, XUV laser-matter interaction will become available at ultra-high intensities. But even tabletop facilities such as XUV lasers or High Harmonic Generation, are starting to reach intensities high enough to produce dense plasmas. XUV laser-matter interaction is studied by a 1D hydrodynamic Lagrangian code with radiative transfer for a range of interesting XUV sources. Heating is found to be very different for $Z = 12-14$ elements having L-edges around the XUV laser wavelength. Possible absorption mechanisms were investigated in order to explain this behaviour, and interaction with cold dense matter proved to be dominant. Plasma sensitivity to XUV laser parameters such as energy, pulse duration, and wavelength was also studied, covering ranges of existing XUV lasers. We found that XUV laser-produced plasmas could be studied using tabletop lasers, paving the way for future VUV-FEL high intensity experiments.

PACS. 52.38.Dx Laser light absorption in plasmas (collisional, parametric, etc.) – 52.65.Kj Magnetohydrodynamic and fluid equation – 42.55.Vc X- and gamma-ray lasers

1 Introduction

The plasma physics community is preparing for a new challenge with the construction of ultra-bright, ultra-fast, tunable XUV sources, allowing experimental plasma studies in unprecedented temperature-density regimes. VUV free-electron lasers (VUV-FEL) such as TTF II in Germany are being built, which will generate highly coherent XUV sources with average brilliances up to 10 orders of magnitude higher than those of third generation synchrotrons [1–3], the most intense sources available yet. These will of course provide extraordinary tools for probing high density and warm or high temperature plasmas, such as those produced in short-pulse laser-plasma interaction [4]. But one of the most intriguing possibilities provided by these new sources, will be direct plasma creation, extending laser-plasma interaction to the sources emitting in the XUV range.

The sources of interest to our case are monochromatic, emitting in the tens to few hundred eV range. This energy domain is referred to as XUV or soft XUV light, and the sources, behaving as lasers, are for the rest of the article called XUV or soft XUV lasers. Close to this interaction regime, only two sets of experiments have been reported up to date, one on Extreme UV FEL-cluster interaction, [5], and the other concerning XUV laser-solid interaction [6,7], at very low intensity (under 5×10^{11} Wcm^{-2}).

Soft XUV laser-plasma interaction studies are indeed an emerging field. The lack of high intensity coherent soft XUV sources, with only one monochromatic XUV source showing sufficient energy output on target to produce a plasma [8], stimulated little theoretical work up to now. But intensity outputs are quickly increasing by orders of magnitude, not only with sources such as forthcoming VUV and XUV-FEL radiation [1–3] but also with upgrades in widespread tabletop XUV sources, with higher energy output and improved focusing XUV optics [8,9]. Highly coherent and brilliant XUV sources generating intensities on target above 10^{13} Wcm^{-2} will soon become available, and the need for modelling of XUV-matter interaction at high flux becomes more urgent.

Although XUV-matter interaction has been a very fruitful field of research, radiation transport has been studied in specific contexts (including Inertial Confinement Fusion or astrophysics) where the XUV radiation producing the plasma is broadband, and blackbody approximations usually hold. With soft XUV laser-plasma interaction, although the radiation is energetic enough that it may interact with bound electrons, energy transport is non-trivial, since the laser is monochromatic.

[a] e-mail: marta.fajardo@ist.utl.pt

The scope of this article is to give a first approach to the hydrodynamic behaviour of XUV laser-produced plasmas. For the rest of this article, only sources emitting in the range from 10 to 100 eV (with wavelengths ranging from 12 to 120 nm) will be considered.

As for any laser-produced plasma, the hydrodynamic evolution results, first, from the fundamental mechanisms regulating the incident laser absorption inside the target. Following visible or infrared laser-produced plasmas, the hydrodynamic behaviour is expected to depend on laser parameters such as pulse duration, energy or intensity on target. Finally, the composition of the target should play a role on the plasma dynamics, basically having a continuous dependence on atomic number Z. More sophisticated studies would take into account the target structure (flat, rough, grooved) or geometry.

In this work, we have studied the evolution of the plasma according to the above parameters, except target structure or geometry, by considering interaction of matter with intense monochromatic XUV bursts. Questions of coherence, polarization and non-linear phenomena such as collective resonant processes will be left for a future work.

We make use of the radiative hydrodynamic code XRAD [10] in order to model the plasma creation and evolution when produced by an intense burst of monochromatic XUV photons. Pulse duration and intensity dependence, at a given wavelength, are investigated, and predictions are made on electron temperature and electron density conditions achieved. We then study the dependence of the characteristic plasma parameters such as electron density and temperature on the XUV laser wavelength and duration.

2 Laser absorption mechanisms at short wavelength

Ideally, the laser absorption by a target should be treated in two phases. The first is the absorption of the laser by the cold, unperturbed target and then by the target having a plasma layer in front of the remaining solid target. Most of the hydrodynamic codes, developed for infrared, visible or UV lasers interaction, consider the plasma creation as instantaneous, at least comparing to the driving laser duration. In this approximation, the laser interacts only with the expanding plasma, since the beam is reflected at the critical density, N_c, typically about a hundred times lower than solid density.

Extension of the traditional models of optical laser absorption to the XUV domain seems difficult. Indeed, for these wavelengths the critical density is more than one order of magnitude higher than solid density, $N_s \sim 10^{23}$ cm^{-3}, meaning that most of the energy deposition is done into the cold core of the target. For example, for a visible ($\lambda = 0.53$ μm) laser, the critical density is $N_c = 4 \times 10^{21}$ cm^{-3} while for a 13 nm XUV laser the critical density rises up to $N_c = 6.5 \times 10^{24}$ cm^{-3}. At a first glance, it appears that a good description of the interaction of XUV laser with cold target is crucial for being able to model the hydrodynamic of this new kind of plasma with a good degree of confidence. A more complete study of the XUV laser absorption mechanisms by the plasma is also necessary.

For under-dense plasmas, we may identify the following mechanisms as the most probable for XUV laser absorption. For the case of visible or infrared lasers, in the absence of resonant non-linear absorption, the main mechanism for light absorption is inverse Bremsstrahlung (IB). The IB absorption A_{IB} [11] is given by:

$$A_{IB} = 1 - I/I_0 = 1 - \exp(-K_{IB}L), \tag{1}$$

where I_0 is the intensity at the plasma entrance and I is the intensity after propagation over a path L and K_{IB} is the absorption linear coefficient given by:

$$K_{IB} = 3.1 \times 10^{-7} Z N_e^2 (\ln \Lambda) T^{-3/2} \omega^{-2} (1 - \omega_p^2/\omega^2)^{-1/2} \tag{2}$$

where Z is atomic charge, N_e is electron density, $\ln \Lambda$ is the Coulomb logarithm, ω and ω_p are the laser and plasma frequencies, respectively.

Although equation (2) considers a simplistic case of homogeneous plasma of density N_e, it gives a first insight for λ-scaling. As one can tell from equation (1), the IB linear absorption coefficient depends on the ratio ω_p/ω, that is to say, to the ratio N_e/N_c. Since for XUV lasers the critical density is about ten times higher than solid density, we may assume that the ratio ω_p/ω is negligible. This is highly different from visible lasers for which most of the incident energy is absorbed near or at the critical density, leading to a ratio of ω_p/ω close to unity. For visible lasers the term $(1 - \omega_p^2/\omega^2)^{-1/2}$ may be quite large, while for XUV laser it is always close to unity, showing that K_{IB} coefficient is strongly reduced when considering XUV lasers. This is also reinforced by the dependence of K_{IB} with wavelength as given by the term ω^{-2} (equivalent to λ^2, λ being the laser wavelength). Finally it appears that although it is often the dominant process for visible laser absorption, the λ-scaling shows that the fraction of energy absorbed by this process is rather low when considering an XUV laser.

Another well-known mechanism for laser absorption is the so-called resonant absorption [12]. Here the laser absorption is due to the energy transfer by resonantly exciting a plasma wave. Therefore, the resonant absorption is really efficient at or near the critical density. As discussed above, the critical density for XUV laser is above solid density. In the absence of strong compression by a shock wave, the XUV laser is never resonant with the plasma wave, making the resonant absorption negligible. The laser light may excite and transfer energy to other waves such has ion acoustic wave or electron waves driven by an ion density fluctuation, mechanisms known as plasma instabilities. Brillouin scattering, as a source of ion acoustic waves, may be considered as negligible at XUV wavelengths. Stimulated Raman scattering (SRS) appears for densities lower than $N_c/4$, which make it a potential mechanism for laser absorption. However, the instability threshold scaling as $I\lambda^2$, I being the laser intensity,

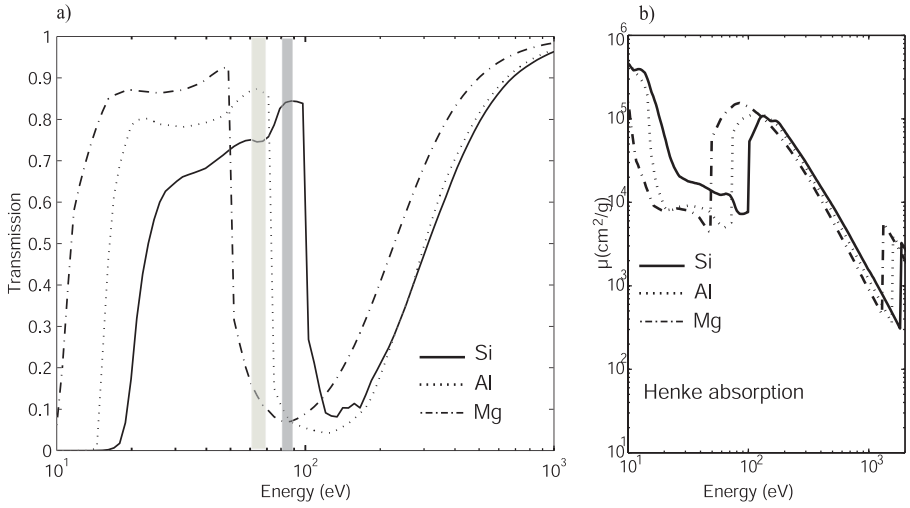

Fig. 1. (a) Transmission as a function of photon energy for 0.1 μm thickness foils of Mg, Al and Si. (b) Corresponding mass absorption coefficients from Henke tables.

the very short wavelength of the XUV laser implies intensities much higher than the ones considered in this work ($10^{11}-10^{13}$ Wcm^{-2}) for producing SRS.

At short wavelength, the laser may interact directly with core levels of the cold target atoms or even of the plasma ions. Absorption of the laser appears here by photo-ionization. Note that such direct single-photon absorption of the laser is generally impossible for visible laser, where multi-photoionization is dominant during the beginning of the interaction and inverse Bremsstrahlung soon takes over. The XUV laser-plasma interaction is then ruled by the absorption coefficient, which is mainly dependent on the atomic physics of the material. A different behaviour for low Z elements can thus be expected. Electron binding energy for the $2p$ electrons is 49.5 eV for Mg, 72.5 eV for Al and 99.5 eV for Si in their natural form, meaning that a 90 eV photon can eject an electron from the $2p$ layer in solid cold Mg and Al, but not Si. This translates into a very different absorption probability of the photons by the cold target. In Figure 1a the transmission of a thin layer (0.1 μm) of Si, Al and Mg is shown, confirming that a Si target is transparent at 90 eV radiation, but not an Al or Mg target. Note that for an XUV laser around 70 eV, the same transparent/opaque transition occurs between elements Al and Mg respectively. The transmission of Figure 1a were calculated from natural opacities, known as Henke absorption coefficients, shown in Figure 1b, that can be found in reference [13].

As previously discussed, the XUV laser will always interact with the bulk of the target, meaning that photo-absorption rules the whole interaction. Photo-absorption is still a major mechanism for XUV laser absorption even considering the hot plasma. The main difference will be in the variation of the photo-absorption cross-section versus photon energy since there is a wide range of ionic species present in a plasma as compared to a solid. In our code, the photo-absorption of cold matter is taken from Henke data, while for hot plasma it is calculated using an average-ion, non-LTE atomic physic code, POTREC [14]. Special care has to be taken for low temperature (warm) dense plasma for which classical atomic codes fail for calculating accurate data. Our straightforward solution was to interpolate the photon absorption for low temperature plasma by using the cold solid target and the hot plasma (above 10 eV) data.

From Henke absorption coefficients shown in Figure 1, it is clear that at 90 eV (13 nm XUV laser), Al and Mg are strongly absorbing, while Si is relatively transparent. Deep penetration of the XUV laser into the solid target is possible in the case of cold silicon and results in bulk heating. Since the energy is deposited over a large volume, we may expect smooth electron density gradients and relatively low electron temperature. In contrast, the absorption lengths in Mg and Al are about 400 Å, that is, of the order of magnitude of the skin depth of visible laser deposition (∼100 Å). Then XUV laser-produced plasma should resemble visible laser-produced plasma regarding temperature evolution, although the density is kept at a much higher level in XUV laser-produced plasmas (a factor of 10 at laser maximum). It appears that atomic number Z dependence in the interaction hydrodynamics at a given XUV laser wavelength is paralleled by wavelength dependence for a given material.

Cold solid photo-absorption can only account for some degree of the plasma heating, since as soon as the plasma is created and heated up, the XUV laser absorption should vary. Comparing Figure 1b and Figure 2a, an increase of the photo-absorption coefficient is found to occur in the energy range of the XUV laser drive. For much higher temperatures such as the one used in Figure 2b, excitations of high principal quantum number, n, become abundant, and ionization by photo-absorption becomes very likely. Indeed, when the plasma becomes sufficiently warm for very stripped ions to become abundant, characteristic absorption lines that correspond to resonant transitions appear. Line coincidence, which is not relevant for the cases studied here, would become important for hard XUV lasers or even XUV laser coupled to lighter elements, and laser deposition into the heated plasma would be strongly dependent on the element.

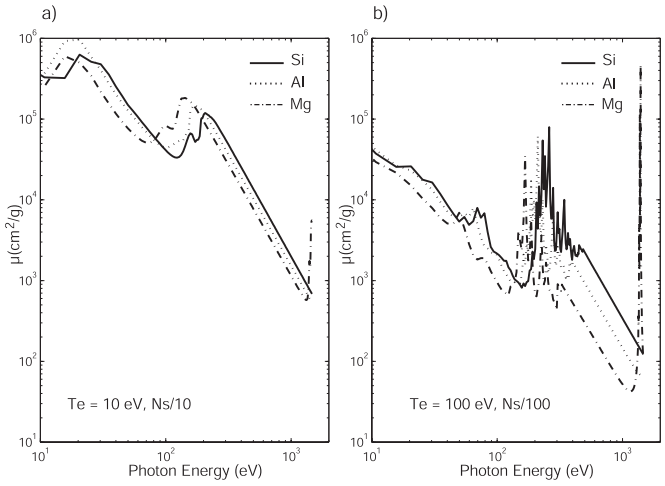

Fig. 2. Mass absorption coefficients for Mg, Al and Si calculated by POTREC. (a) Average ion absorption at 10 eV and 1/10th of solid density. (b) Absorption at 100 eV and 1/100th of solid density.

3 Numerical simulation of plasma creation with an XUV laser

In this section, we will numerically investigate the general features of plasma creation by means of intense and monochromatic source in the XUV range. For the present work, XUV laser interaction with matter is described using XRAD [10], a 1D hydrodynamic code, that includes radiation transport and non-LTE atomic physics using a time-dependent average-ion model [14]. The code was initially designed for the study of radiatively heated foils, using broadband XUV sources as heating pulse for opacity measurement experiments [15]. Radiation transport is taken into account using the multi-group method [16]: the photon energy spectrum, ranging from visible to hard XUVs, is integrated into discrete energy groups, for which Planck and Rosseland mean opacities are calculated based on the absorption coefficients calculated by POTREC. The transport equation is then solved between each Lagrangian plasma cell [17], and energy re-distribution inside the plasma is thus taken into account. Classical electron thermal conductivity is included.

Some modifications were necessary in order to simulate the interaction with a monochromatic XUV laser beam. The temporal profile of the beam was taken from XUV lasers simulations that indicated close to Gaussian time evolution. The energy spectrum of the incident radiation was divided into energy groups with higher resolution around and at the XUV laser energy. For our case, we used 10 eV groups around the XUV laser energy and the L absorption edge energies of the materials we have studied (80–150 eV), and increased the groups geometrically outside the XUV laser region. This 10 eV spectral resolution was low enough that the energy transfer calculations were kept at a reasonable computing time, while keeping the characteristics of the absorption for different materials, as confirmed in Figure 1, where the spectral regions of interest have been highlighted.

Figure 3 shows a map of the electron temperatures and densities, respectively for different targets, in the case of an XUV laser (90 eV, 13 nm), with Gaussian pulse duration of 10 ps at FWHM, and intensity on target of 10^{13} W/cm^2. This is a relevant soft XUV laser wavelength and duration, currently being optimized experimentally because of the XUV nanolithography applications [18]. We chose three targets of 10 μm thickness with consecutive atomic number, Mg, Al and Si (respectively $Z = 12$, 13 and 14). The XUV laser comes form the right, reaching its maximum intensity at $t = 0$. The surface is set at the origin, the original target ranges from -10 μm to 0. Electron temperature and density are shown evolving as a function of time and position in Cartesian coordinates. At this intensity and time duration, an energy density of roughly 100 J/cm^2 is deposited on target.

The most striking feature in Figure 3 is the difference in the hydrodynamic behaviour and plasma characteristics between Si and the other two elements. For Mg and Al, we find the well-known pattern of laser deposition into the target surface layer, the plasma being heated along the laser pulse. While the XUV laser pulse is on (-5, $+5$ ps), the heated layer is smaller than 0.2 μm in thickness for both targets. The peak temperatures are in the same range: about 65 eV for Mg and 45 eV for Al. The slight change in peak temperature from Mg to Al comes from the weak differences in absorption coefficient at 90 eV that were shown in Figure 2a. The plasmas expand at velocities of the order of 10^7 cm/s, cooling down at a rate of 2 eV/ps, and generating a shock wave of density superior to solid (reaching 2.1 times N_s in the case of aluminium and 1.93 times N_s in the case of magnesium) that penetrates into the target. After the XUV laser pulse is interacting with the target (time longer than +5 ps), the bulk of the target is ionized by thermal conduction and radiative transfer. About 50 ps after the peak of the laser the plasmas extend from about 4 μm inside the target, up to 8 μm outside. For the Si plasma, however, there are no steep gradients, since the laser penetrates deeply into the core of the target from the very beginning of the interaction. The initially heated part is from 7 to 10 μm to be compared to a small fraction of μm in case of Mg or Al. The heating is less effective, electron temperature stays below 15 eV, and the density is also very homogeneous, keeping smooth gradients. Therefore the cooling is also less abrupt with a rate of 0.15 eV/ps. Finally, it is interesting to note that the weak differences in absorption coefficients (see Fig. 2) between Al and Mg at 90 eV are reflected in a comparable behaviour of the two plasmas.

The Z-dependence of the target for a given XUV laser wavelength is comparable to the wavelength dependence for a given material. Figure 4 shows the result of a simulation of an XUV laser of 60–70 eV interaction with solid aluminium target, in the same conditions as Figure 3b. The behaviour of the Al plasma is now very similar to the Si plasma in Figure 3c, with the characteristic bulk heating and low temperatures of transparent materials.

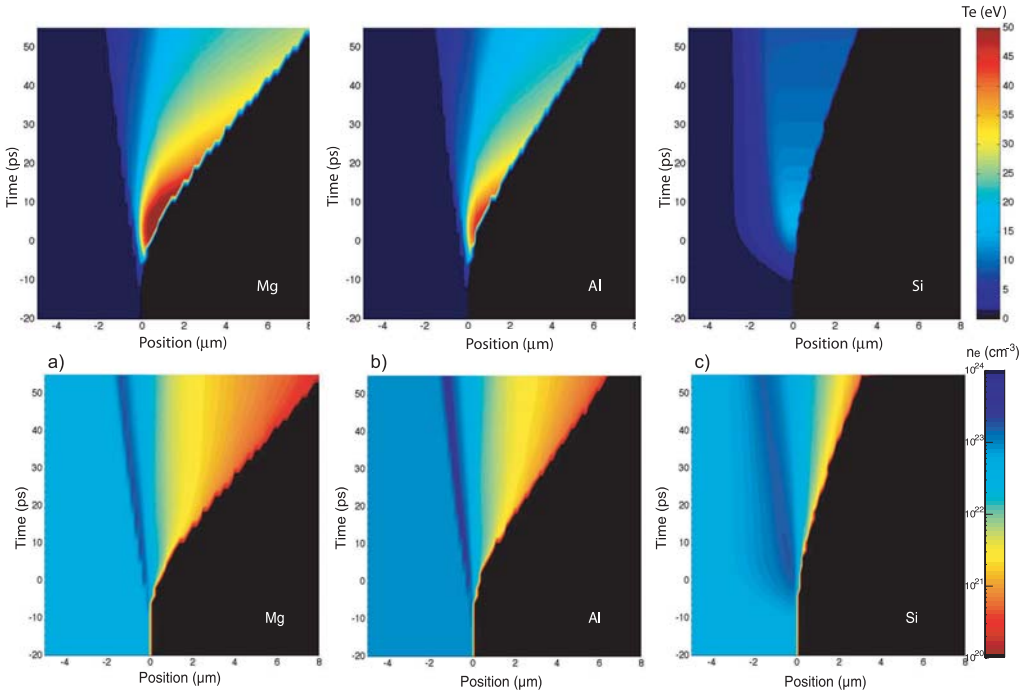

Fig. 3. Top: electron temperature (eV) and density (cm^{-3}) for Mg, Al and Si plasmas created by a 90 eV, 10 ps duration, 10^{13} Wcm^{-2} on-target intensity XUV laser, as a function of time and space. Ripples in the plasma-vacuum interface are due to the finite size mesh used in the numerical code. Laser maximum at $t = 0$ and target thickness 10 μm. Temperature scale is kept constant to enhance the different plasma characteristics.

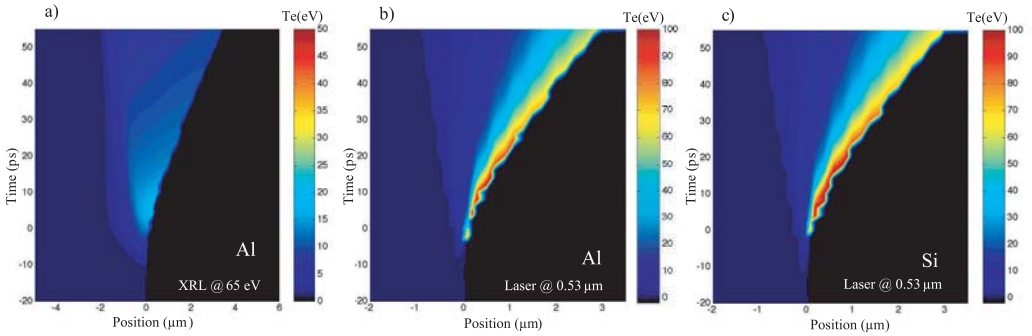

Fig. 4. Comparison of different laser-solid interactions. Target is 10 μm thick, laser maximum at $t = 0$ at an intensity of 10^{13} Wcm^{-2} and 10 ps pulse duration. (a) XUV laser energy is 65±5 eV and target is Al; (b) and (c), interaction with visible laser ($l = 0.53$ μm) is shown for Al and Si, respectively.

Since absorption is of the same order of magnitude for all elements as soon as the plasma is heated, it might be surprising to find that cold solid photo-absorption has durable influence in the plasma hydrodynamic behaviour. However, coupled to the fact that IB absorption is kept negligible at lower densities, direct photo-ionization becomes less probable as the plasma heats, and is down by a factor of 2 at 10 eV and by more than a factor of 20 at 100 eV, so that a large fraction of the XUV laser energy is still being dumped at solid density, inside the cold target, while the plasma is heated.

Further heating can be explained by electron thermal conductivity and inverse Bremsstrahlung, both mechanisms included in the code. The gradients being smoother than for classical laser deposition, thermal conductivity does not play as important a role. Energy coupling into the free electrons by inverse Bremsstrahlung is also less efficient as mentioned above, but this effect is compensated by higher electron density at comparable temperatures. The plasma gradients being very smooth, laser deposition is made for a long plasma distance, and heating of the plasma comparable to visible lasers is achieved. These two effects, however, are only important in the case of high densities coupled to high temperatures guaranteed by an effective photo-absorption, and remain negligible for transparent materials.

These features are in contrast with the plasma parameters found in visible laser-matter interaction. Shown in

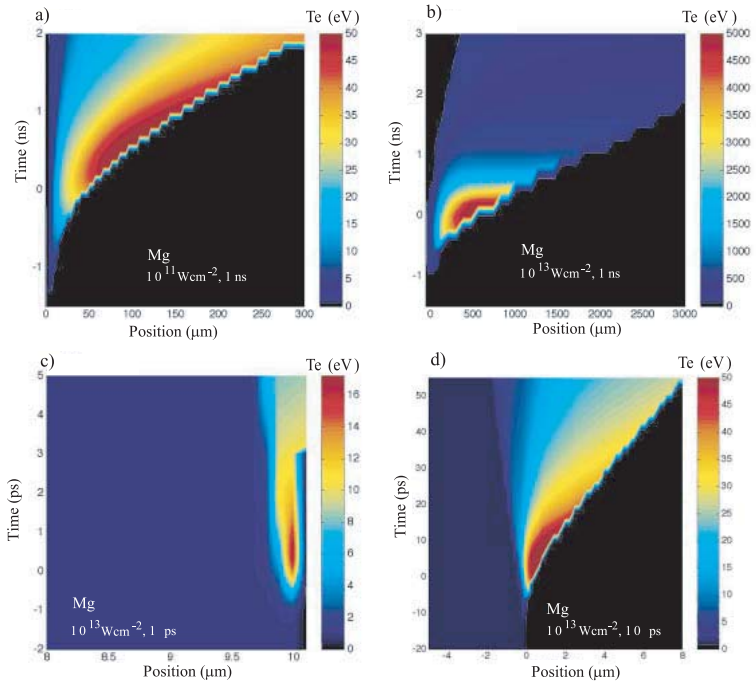

Fig. 5. Electron temperature as a function of time and space for Mg target. 90 eV XUV laser maximum at $t = 0$ and target thickness 10 μm. Intensity on target is 10^{11} W/cm^2 for 1 ns pulse duration (a), and 10^{13} W/cm^2 for(b), (c) and (d), for pulse durations 1 ns, 10 ps and 1 ps respectively. Note the different scaling in time and distance to the target surface for each simulation.

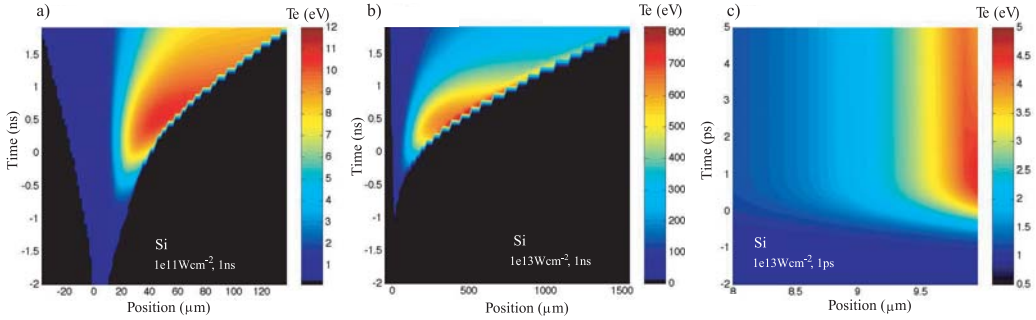

Fig. 6. Electron temperature as a function of time and space for Si target. Again, 90 eV XUV laser intensity on target is 10^{11} W/cm^2 for 1 ns pulse duration in (a), and 10^{13} W/cm^2 for (b) and (c), for pulse durations 1 ns, and 1 ps respectively.

Figures 4b and 4c are the XRAD calculation of electron temperature for aluminium and silica respectively, using a 0.53 μm laser at 10^{13} Wcm^{-2} and 10 ps pulse duration, as in the previous case. As expected, the hydrodynamic heating and expansion is similar for both materials. The main absorption mechanism is in this case inverse Bremsstrahlung, and no abrupt Z-dependence on the target material can be found. The temperatures and densities found with visible laser interaction are indeed comparable to the interaction of an XUV laser with an opaque material, with slightly higher temperatures and lower densities due to a more efficient coupling at $N_c \sim 10^{-2} N_s$.

4 Hydrodynamic behaviour of XUV laser-produced plasmas

Hydrodynamic parameters' dependence of the XUV laser–produced plasma on irradiation conditions was also studied. Simulations were run at different irradiation conditions, shown in Figures 5 and 6, for Mg and Si. XUV laser energy was kept at 90 eV. We first studied the energy dependence by varying the intensity on target from 10^{11} W/cm^2 up to 10^{13} W/cm^2 and keeping pulse duration at 1 ns. This is the characteristic emission times for the most energetic tabletop XUV lasers [19]. Influence of pulse duration on plasma characteristics was also studied by varying the pulse length from 1 ps, to 10 ps and 1 ns while keeping the intensity constant at 10^{13} W/cm^2. Again for all the modelling, the target thickness is 10 μm and the outer surface is set at 0. The XUV laser is coming from the right.

In Figures 5a and 5b are shown the time and space evolution of the electron temperature for Mg targets irradiated at intensities of 10^{11} Wcm^{-2} and 10^{13} Wcm^{-2}, respectively. The overall plasma characteristics are very different. At 10^{13} Wcm^{-2}, the peak electron temperature is as high as 5 keV while the temperature remains quite low (55 eV) at 10^{11} Wcm^{-2}. Note that the ratio of the temperatures ($\sim$100) between the two runs is quite close from

the ratio on laser energies (100), indicating that there is no strong difference on laser absorption. On the first glance, this is surprising as the plasma should be quite transparent due to the fact that the critical density is about ten times the solid density. This confirms that the coupling between XUV laser and target is very efficient, because, as we discussed previously, energy dumping is made at the core of the target and on a very thin layer.

The differences in peak temperatures lead to a strong change on plasma expansion (3000 μm at the highest intensity compared to 250 μm at 10^{11} Wcm^{-2}), since the sound speed varies as $Te^{1/2}$. The cooling rates are quite different in the two cases. Indeed, at higher intensity, the plasma cools down very quickly, from 5 keV at $t = 0.4$ ns down to less than 1 keV at $t = 1.5$ ns. Also the peak temperatures remain only as long as the XUV laser is irradiating the target. However, on the low intensity case, the outer plasma layer remain at same temperature of about 50 eV even 0.5 ns after the XUV laser has been switched off.

The dependence of the plasma characteristics with pulse duration might be first studied by comparing the cases 1 ns, 10^{11} Wcm^{-2} [Fig. 5a] and 10 ps, 10^{13} Wcm^{-2} [Fig. 5d], as the energy density on target is kept constant. As previously pointed out, peak temperature is to a first approximation proportional to the energy density deposited on target: the temperatures reached at 10^{13} W/cm^2, $\Delta t_{XRL} = 10$ ps (65 eV) and 10^{11} W/cm^2, $\Delta t_{XRL} = 1$ ns (55 eV) are of the same order of magnitude. Consequently, we should expect to get the same sound speed and then plasma sizes different by about two orders magnitude as coming from the ratio on pulse duration. Indeed, plasma expands over 250 μm for 1 ns irradiation while it is as low as 2 μm for 10 ps pulse.

For the very short pulse (1 ps, Fig. 5c) laser-produced plasmas, the peak temperature reached is very low (16 eV), with an energy density of only 10 J/cm^2 on target, and there is almost no expansion into vacuum, energy dissipation being made by thermal conduction into solid target. This is very different from long pulse case where very high temperatures are reached, and the plasma expands for several hundred to several thousand of microns.

In Figures 6a to 6c, the same results of calculation as shown in Figures 5a to 5d are displayed, but with a silicon target instead of magnesium. Direct comparison of Figures 5 and 6 clearly shows that the influence of the cold target absorption is quite important and may even dominate the interaction in the case of very short pulses (1 ps). Indeed, plasma characteristics are much more different than what we would expect with a classical Z-scaling. For example, although the peak temperature scales again nearly as the laser energy, we may observe that the peak temperature reaches 800 eV for run 1 ns, 10^{13} Wcm^{-2} (Fig. 5b), when we would expect 1 keV by scaling from the run of 1 ns, 10^{11} Wcm^{-2} (Fig. 5a). Again due to the change on cold target absorption, for all the cases and considering the same irradiation condition, the peak temperature is about 4 to 7 times lower for silicon plasma than for magnesium. This is even most evident in the silicon plasma, where we can see in Figure 5a the expansion of the back of the target, which initially is 10 μm thick. Deep penetration of the XUV laser in silicon target is also visible in Figure 6d where the bulk is heated over more than 2 μm while on Mg, the heated layer is as small as 0.2 μm. It is worth noting that irradiating a target that is transparent at the XRL wavelength created plasma conditions that are quite close to the so-called "warm dense matter" (near solid density and few eV temperature). This is observable on runs displayed in Figure 3c (10 ps, 10^{13} Wcm^{-2}) and Figure 6c (1 ps, 10^{13} Wcm^{-2}).

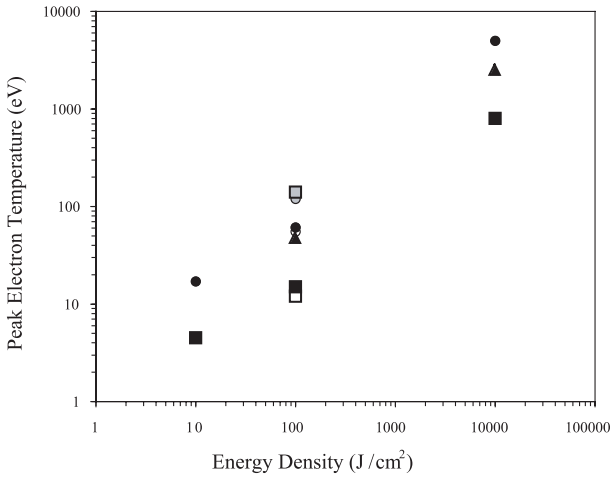

Fig. 7. Peak electron temperatures for Al (triangle), Mg (dot) and Si (square), as a function of energy density on target, for 90 eV laser at 10^{13} Wcm^2 (black), 10 ^{11} Wcm^2 (grey) and visible laser at 10^{13} Wcm^2 (open symbol).

The dependence on the heating conditions is summarized more explicitly in Figure 7. Peak electron temperature for each simulation is shown as a function of energy density on target, for different targets and laser parameters. Almost an order of magnitude difference is kept between the Mg and Si targets at 90 eV XUV laser. This difference is consistently repeated for different laser intensities and pulse durations, but is non-existent for visible laser produced plasma.

5 Discussion

Since the plasma is radiatively heated, the exactness of the opacity calculations used in the radiative transfer equations becomes a key issue. Low-temperature, high density opacities, that are most relevant for XUV laser absorption, are very poorly known. The non-LTE average ion model we used, as all other atomic physics models, does not converge properly for low temperature and high density. To give physically consistent results, we have thus interpolated the opacities between two valid regimes, namely between Henke tables for natural absorption and 10 eV, $N_s/10$ plasma. This does not change the validity of the gross features, because of the arguments given in Section 2 for laser deposition into the solid target, but might give some error bars on the temperature.

Other improvements involve the use of time-dependent atomic physics, which are especially needed for short-pulse interaction, when laser duration becomes of the order of the electron-ion collision, excitation and collision times. Extension to the ultra-short pulse domain, that will become possible with VUV-FEL radiation, should keep the characteristic differences in plasma temperatures seen in Figure 7. Short-pulse interaction could reinforce this behaviour, since the energy deposition would be faster than thermalization times. This can only be accounted for with a time-dependent collisional-radiative model, valid for low temperatures and high densities, well beyond the scope of this work. Again, these improvements would only account for a more accurate description of the ionization, but should not change the coarse differences between close-Z elements of highly transparent or absorbent nature.

Finally, the model is one-dimensional, so temperature is overestimated for long times, away from the target surface. This is very well-known from the visible laser-matter simulations, and can accounted for by a rough 1/3 energy loss due to lateral expansion. As always, a bi-dimensional code would be more accurate.

6 Conclusion

We have seen striking differences in the plasma heating for a given XUV laser, according to target material, that are equivalent to different heating of the same material for a tunable XUV laser. These are justified by the absorption mechanisms at stake and, as we have shown, photoabsorption is predominant. The hydrodynamic behaviour is to a first approximation dependent on the Henke absorption coefficients, making the target transparent or strongly opaque to the XUV laser wavelength.

We are in need of atomic physics data in order to improve our model, but the way to produce warm-dense-matter in laboratory is precisely by achieving XUV laser-matter interaction, making it a closed-loop problem. A well-characterized laser-plasma interaction experiment would benchmark our code. There are examples of short-pulse visible laser-plasma experiments on thin foils that have reached warm and very dense plasmas, probed by absorption and emission spectroscopy [20]. The time evolution of the plasma however, may complicate the interpretation of the results, so ultra-intense, short-pulse, tunable VUV-FEL's are needed to make opacity benchmarks in warm dense matter.

In conclusion, XUV laser matter interaction was studied for several irradiation conditions. It was found that the plasma evolution is strongly dependent on the target material. For a transparent material and a relatively short pulse, a warm, high density plasma, with very smooth gradients can be obtained. As an example, bulk heating of the material is achieved in the case of a silicon plasma, even with such low intensity (10^{13} Wcm^{-2}) and photon energy (90 eV) as considered here. This warm dense matter is found in a large plasma region (>10 μm) and lasts for a sufficient long time (larger than recombination and collision times) to potentially lead to a quasi-equilibrium state of highly correlated plasma.

From our simulations, ablation is completely distinct to what is known in visible laser-produced plasmas. This is a very challenging perspective, and we are looking forward to the XUV-laser focusing experiments to achieve these new interaction regimes.

One of us (M.F.) was financed through FCT (Portugal) under the program POCTI, with Contract number SFRH/BPD/11235/2002.

References

1. R.F. Service, Science **298**, 1356 (2002) (in News)
2. A. Cho, Science **296**, 1008 (2002) (in News Focus)
3. N. Patel, Nature **415**, 110 (2002) (News Feature)
4. R. Lee et al., J. Opt. Soc. Am. B **20**, 4 (2003)
5. H. Wabnitz, L. Bittner, A.R.B. de Castro, R. Döhrmann, P. Gürtler, T. Laarmann, W. Laasch, J. Schulz, A. Swiderski, K. von Haeften, T. Möller, B. Faatz, A. Fateev, J. Feldhaus, C. Gerth, U. Hahn, E. Saldin, E. Schneidmiller, K. Sytchev, K. Tiedtke, R. Treusch, M. Yurkov, Nature **420**, 482 (2002)
6. L. Juha, A.R. Präg, J. Krasa, A. Cejnarová, B. Kralikova, J. Skala, D.Chvostova, V. Vorlicek, J. Krzywinski, A. Andrejczuk, M. Jurek, D. Klinger, R. Sobierajski, H. Fiedorowicz, A. Bartnik, L. Pína, J. Kravarik, P. Kubes, Yu.L. Bakshaev, A.S. Chernenko, V.D. Korolev, M.I. Ivanov, M. Scholz, L. Ryc, K. Tomaszewski, R. Viskup, F.P. Boody, AIP Conf. Proc. **641**, 504 (2002)
7. B.R. Benware, A. Ozols, J.J. Rocca, I.A. Artioukov, V.V. Kondratenko, A.V. Vinogrado, Opt. Lett. **24**, 1714 (1999)
8. S. Le Pape, Ph. Zeitoun, M. Idir, P. Dhez, J.J. Rocca, M. François, Phys. Rev. Lett. **88**, 183901 (2002)
9. M. Fajardo, P. Mercère, G. Faivre, Ph. Zeitoun, S. Kazamias, C. Valentin, D. Douillet, F. Augé, L. Antonucci, Ph. Balcou, private communication
10. C. Chenais-Popovics, J.-C. Gauthier, F. Puech, P. Renaudin, L. Visconti, SPIE Proc. **2015**, 220 (1994)
11. J.W. Johnston, J.M. Dawson, Phys. Fluids **16**, 722 (1973)
12. W.L. Kruer, *Physics of laser Plasma interactions* (Addison-Wesly Publishing Company, 1988)
13. B.L. Henke, E.M. Gullikson, J.C. Davis, At. Data Nucl. Data Tables **54**, 181 (1993); for updated values see `http://www-cxro.lbl.gov/optical_constants/`
14. A. Mirone, J.-C. Gauthier, F. Gilleron, C. Chenais-Popovics, J. Quant. Spectr. Radiat. Transfer **58**, 791 (1997)
15. C. Chenais-Popovics, F. Gilleron, M. Fajardo, H. Merdji, T. MiBalla, J.C. Gauthier, P. Renaudin, S. Gary, J. Bruneau, F. Perrot, T. Blenski, W. Folsner, K. Eidmann, J. Quant. Spectr. Radial. Transfer **65**, 117 (2000) and references therein
16. R. Ramis, R. Schmalz, J. Meyer-ter-Vehn, Comp. Phys. Comm. **49**, 475 (1988)
17. D. Mihalas, B. Mihalas, *Foundations of radiation hydrodynamics* (Oxford University Press, New York)
18. J. Dunn, Y. Li, A.L. Osterheld, J. Nilsen, J.R. Hunter, V.N. Shlyaptsev, Phys. Rev. Lett. **84**, 4834 (2000)
19. J.J. Rocca, Rev. Sci. Instrum. **70**, 3799 (1999) and references therein
20. P. Audebert, R. Shepherd, K.B. Fournier, O. Peyrusse, D. Price, R. Lee, P. Springer, J.-C. Gauthier, L. Klein, Phys. Rev. Lett. **89**, 265001 (2002)